COBEM 2023 27TH INTERNATIONAL CONGRESS OF MECHANICAL ENGENEERING

ABCM Brazilian Society of Mechanical Sciences and Engineering
27th ABCM International Congress of Mechanical Engineering
December 04-08, 2023, Florianópolis-SC, Brazil

COB-2023-0572
FLUID DYNAMICS ANALYSIS OF A MICRO HORIZONTAL AXIS WIND TURBINE

Guilherme Vicente Toquini
Celso Antonio Bittencourt Sales Junior
Felipe Eduardo de Farias
Angie Lizeth Espinosa Sarmiento
Diego Mauricio Yepes Maya
Universidade Federal de Itajubá, Av. BPS, n1303, bairro Pinheirinho, Itajubá, Minas Gerais
guilhermetoquini@unifei.edu.br, celsosalesjunior@unifei.edu.br, angieespinosa@unifei.edu.br, diegoyepes@unifei.edu.br

Abstract. *Micro wind turbines are turbomachinery usually with rotor diameters smaller than 2.5m, they are ideal for generating electricity in locations with weak/moderate winds and in isolated locations of the grid. In this context, simulations of computational fluid dynamics (CFD) are often being used to predict the aerodynamic performance of this type of machine, given recent technological and computational capabilities developments. Thus, the present study aims to predict the performance of the micro horizontal axis wind turbine (micro HAWT) present in the Laboratory of Renewable Sources and Solar Energy of the Federal University of Itajubá, through a methodology developed using the ANSYS® software. So it was possible to predict the torque and efficiency of the turbine for different rotations degrees, describing its characteristic curve and developing a fast response methodology for predicting the aerodynamic performance of small HAWTs.*

Keywords: *Micro HAWT, CFD, Wind energy, Power coefficient, Tip Speed Ratio.*

1. INTRODUCTION

The consumption of electricity serves as a significant metric for measure a nation's development, as it goes beyond economic growth also reflects the improvement in the quality of life for its population (IEA, 2017). This correlation becomes evident when considering that countries with higher energy consumption have the highest GDP (Gross Domestic Product) per capta. That said, projections for 2050 indicate that electricity demand will increase from 20.204 TWh/year to 41.508 TWh/year, which would imply the doubling of electric power generation enterprises (IRENA, 2019). Therefore, it is crucial to analyze the composition of the current global energy matrix, where in 80% of production stems from non- renewable sources, implying a huge environmental impact, since energy consumption is one of the main causes of climatechange and the emission of Greenhouse Gases (GHG) (UN General Assembly, 1948).

Given this scenario, the promotion of renewable energies has been gained significant interest worldwide through political measures and international agreements leading to an accelerated development of sustainable energy. The global installed capacity of renewable energy witnessed a remarkable growth of 45% between 2010 and 2020, reaching 2.799 GW (IEA, 2018). In addition, the expected employment of renewable energies indicates a high growth trend. Among the renewable energy sources, wind energy is one of the most used, having reached an installed capacity of 743 GW in 2020. Furthermore, projections indicate a remarkable expansion on wind energy capacity with expectations of multiplying its installed capacity by nearly ten times between 2018 and 2050 (IEA, 2018).

In details, wind energy harnesses the kinetic energy of the wind and converts it into useful shaft power for electricity generation. Energy conversion devices in wind energy are generally classified based on the orientation of their rotation axis, namely Horizontal Axis Wind Turbine (HAWT) and Vertical Axis Wind Turbine (VAWT) (Trentin et al., 2022). In particular, micro HAWT are a type of turbomachinery with a maximum diameter of 2.5 m and are an emerging technology that has proven to be an interesting option for small-scale renewable energy generation, especially in urban areas (Stathopoulos et al., 2018), since conventional wind turbines require areas with high wind incidence and vast space for installation (Murali et al., 2017). In addition, the use of micro wind turbines combined with distributed electricity generation can contribute to the universalization of electrification, given that about 840 million people in the world still do not have access to electricity (Gifford, 2010).

For the design of HAWTs, an essential analysis is the prediction of their aerodynamic performance. For this type of study, the CFD (Computational Fluid Dynamics) simulation is a powerful tool, being considered the most efficient and economical method (Shirzadeh et al, 2021). Many CFD approaches use the fluid domain only for one turbine blade, i.e., the simulation is performed in only one of the flow channels, using a rotational periodicity boundary condition, from a non-inertial reference frame (MRF – Moving Reference Frame), which simplifies the annalysis by not using the complete

geometry of the rotor. An example of this can be seen in reference (Hsiao et al., 2013), where a simulation methodology was developed in the ANSYS Fluent ® software from a hexahedral mesh with about 2.6 million elements, subdivided into two zones, one rotating (RZ) and the other stationary (SZ). The simulation produced results that successfully predicted HAWT performance, where the results were close to experimental data and codes based on Blade Element Momentum (BEM) theory.

The Detached Eddy Simulation (DES) model can also be applied to the same fluid domain configuration mentioned above. For instance, a non-permanent configuration was employed in the STARCCM+ software by Rasam et al. (2018), utilizing a polyhedral mesh comprising 70% of the elements in the RZ, with prismatic layers encompassing the blades, resulting in a total of 40 million elements. The predicted aerodynamic performance demonstrated consistency with BEM codes, indicating the considerable potential of the DES method for HAWT simulation. However, it's important to note that the method demands significant computational resources and leading to increased simulation time.

Finally, the study of Shirzadeh et al. (2021) presents a methodology similar to Hsiao *et al.* (2013), but faster, so was defined as the reference of the present study. In this context, the objective of the current study is to validate, complement and apply the methodology proposed by Shirzadeh et al. (2021) in order to predict the aerodynamic performance of a micro HAWT from the Laboratory of Renewable Sources and Solar Energy of the Federal University of Itajubá, through the analysis of its Coefficient of Power (*Cp*) and Tip Speed Ratio (*TSR*).

2. METHODOLOGY

In order to overcome high computational costs, the RZ is composed by an unstructured tetrahedral mesh , with prismatic layers in the region of the blades, and the fluid domain is discretized by a structured mesh only in the SZ, which, coupled with the Reynolds averaged Navier-Stokes (RANS) approach and the k-ω SST turbulence model, resulted in a mesh containing about only 5.6 million elements.

The methodology is divided into three main steps: rotor geometry modeling, mesh generation, and solver setup. The approach involves utilizing two subdomains and simulating a single channel of the turbine rotor. This strategyaims to minimize the number of elements discretized by the Finite Volume Method (FVM), resulting in reduced simulation time and the computational resource requirements. The wind incidence velocity remains constant while the angular velocity of the turbine varies at each simulation, leading to distinct operational conditions characterized by different *TSR*s. Consequently, for each operational condition, the turbine's *Cp* is measured, so enabling the construction of its characteristic curve. Equations (1) and (2)represent the mathematical expression for *Cp* and *TSR*, respectively.

$$Cp = \frac{T\omega}{\frac{1}{2}\rho A {U_\infty}^3} \tag{1}$$

$$TSR = \frac{T\omega}{U_\infty} \tag{2}$$

Where *T, ω, A and R*, the torque, the angular velocity, the area swept and the radius of the HAWT respectively, and ρ and U_∞, the specific mass and flow velocity of the air.

As an methodology improvement, was implemented the use of dimensionless numbers as *GRV* (Grid-Reduced Vorticity)and y^+, to evaluate the degree of refinement of spatial discretization: the first, established by Balduzzi et al. (2016), specifically for simulations of a Darrieus-H VAWT of small size, basically deals with dimensionless value of vorticity and thus estimates the velocity variation within a mesh volume, indicating the adequacy of the prediction of velocity gradients in a given region; the second, named as dimensionless distance to the wall, it is a criterion for which a certain maximum value is required, depending on the turbulence model employed, to perform the appropriate discretization in the region of the boundary layer of the problem. Thus, as in the present study the k-ω SST turbulence model was used, the maximum recommended value of y^+ is 1. Equations (3) and (4) mathematically express these dimensionless numbers.

$$GRV = \frac{\omega_V}{V_o/L_o} \tag{3}$$

$$y^+ = \frac{y u_t}{\nu} \tag{4}$$

Where ω_V represents the vorticity, V_o the local speed, V_o the representative length, y^+ the absolute distance from the wall, u_t the friction velocity and ν the kinematic viscosity of the fluid.

2.1 Validation

To perform the validation of the methodology, the same geometry used in the reference study by Shirzadeh et al. (2021) was constructed and simulated with the same settings of the solver and the same parameters for the computational domain for all the conditions of *TSR*. The results are presented on Figure 1.

Observing Figure 1, it is possible to notice that the characteristic curve constructed by the authors was similar but a little displaced in relation to the reference study. The condition of nominal *TSR* (3.5) was the point with the lowest percentage error, only 11%, an acceptable value. As we move away from the nominal condition, the tendency is for a greater difference, but the largest percentage error, both calculated and visually observed, was at the point of *TSR* = 2, in which there were numerical instabilities during the simulation.

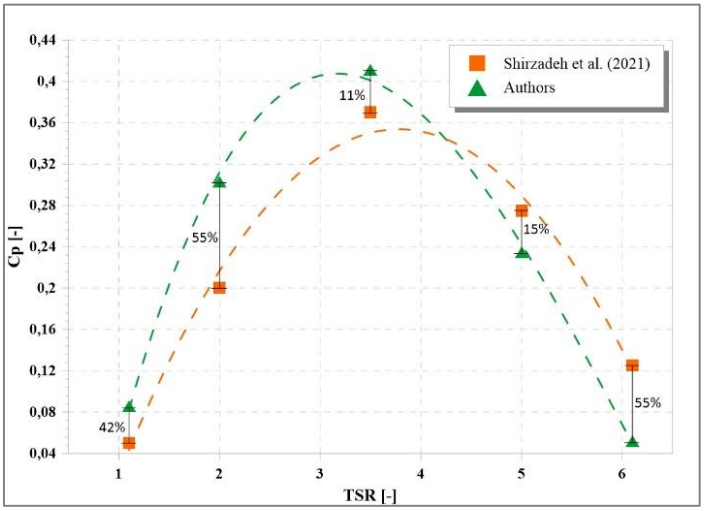

Figure 1: Comparison and percentage error between the characteristic curves by Shirzadeh et al. (2021) and the one constructed by the authors.

Thus, considering the circumstances of the lack of information provided by the reference about the turbine geometry and the natural differences between the cases studied, the methodology could be defined as validated.

The results of the dimensionless number calculations are shown in Figure 2 and were very satisfactory. The *GRV* number was higher for the smaller *TSRs*, what is consistent with the fact that at lower rotations the vorticity is greater. As for y^+, the values were close and, in most simulations, lower than 1, which are very consistent results because the turbulence model used was the k-ω SST too. Thus, it was possible to conclude that to improve future simulations, a beneficial strategy would be to use more refined meshes for higher *TSRs*, something that will be done in the future.

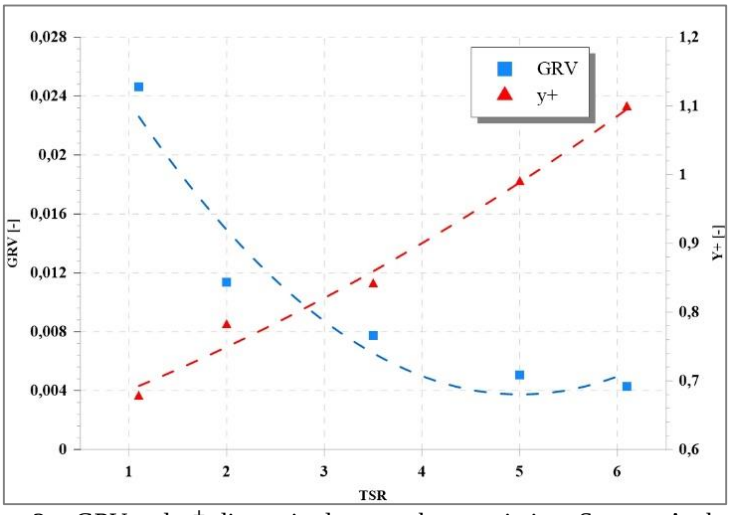

Figure 2 – *GRV* and y^+ dimensionless numbers variation. Source: Authors.

2.2 Geometry and computational domain

The geometry was designed on ANSYS SpaceClaim® software (Figure 3(b) and (c)) and represents a simplified geometry of the blade of the micro HAWT presents in the Laboratory (Figure 3(a)). The turbine has 500 mm of diameter and the blade has an average chord of 59 mm (linear distribution). On the analysis was used the rotor with 3 blades.

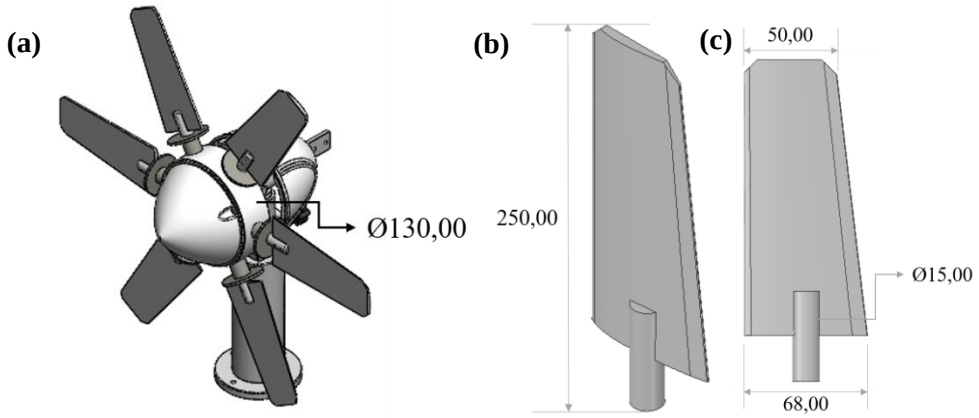

Figure 3: Geometry of the turbine, but with 6 blades (a) and blade used on the simulations (b, c). Source: Authors.

The fluid domain corresponds to a 120° sector section of the main flow through rotor and is divided into two subdomains: Rotating Zone (RZ) and Stationary Zone (SZ). The domain extension was determined from the dimensions specified by Shirzadeh et al. (2021), as well as the boundary conditions, which can be observed in Figure 4.

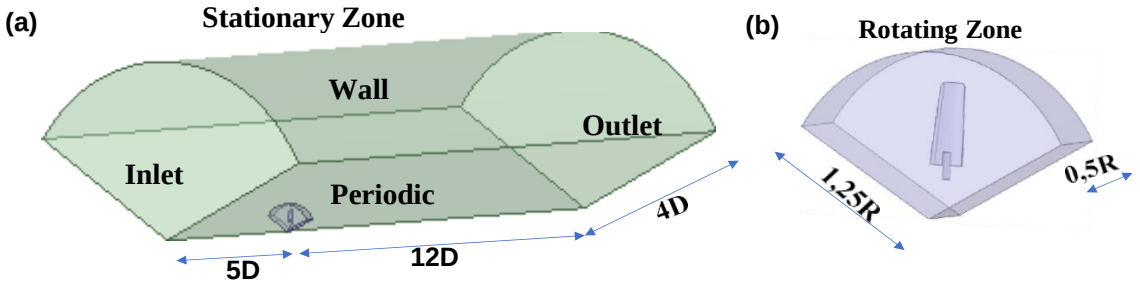

Figure 4: Computational domain and boundary conditions. (a) SZ. (b) RZ. Source: Authors.

2.3 Wind velocity definition

Before starting the mesh generation, the wind incidence velocity to be used in the simulations was defined in order to determine the *TSR* of the first analysis, which will serve as the basis for the subsequent ones. So, through experimental tests of the micro turbine carried out by other authors in the same laboratory, the velocity that resulted in the highest *Cp* curve was 5.92 m/s and the maximum *Cp* was obtained at a TSR of 5.33.

Therefore, in the present study the characteristic curve of the micro HAWT will be described for a speed of 5.92 m/s and the *TSR* point equal to 5.33 will be the first of the curve to be described. Thus, the mesh obtained will serve as the basis for discretization made in the other *TSR* conditions.

2.4 Mesh

The spatial discretization was performed from different approaches in the two zones of the computational domain. The RZ mesh was generated by the ANSYS Fluent Meshing® software, using tetrahedral elements, configuringan unstructured mesh, except in the region near the boundary layer, which was discretized by layers of prismatic elements. For SZ, the *ANSYS ICEM CFD*® software was used to build a structured mesh with hexahedral elements, in order to reduce the total number of elements and obtain the convergence of the simulation more quickly.

Also according to the recommendations of Shirzadeh et al. (2021), for the generation of the mesh in the SZ it was used an approach that segregates it into different blocks ("blocking"), which in turn are automatically generated by the ANSYS ICEM CFD® software. In this mesh generation method, is defined the number of divisions for each edge of the fluid domain. The respective quantities used can be seen in Figure 5(a), and the similar and parallel edges have the same

number of divisions.

The mesh quality metrics evaluated were skewness, orthogonal quality and determinant, for which the minimum values recommended by ANSYS® software are close to 0.3, 0.02 and 0.4, respectively. Thus, to meet these values, a rounding with 7 mm of radius was performed on the meeting edges of the periodic faces, which can be seen in details onFigure 5(b). The result of the spatial discretization of the SZ was a mesh with 1,3 million elements and is presented in Figure5(c).

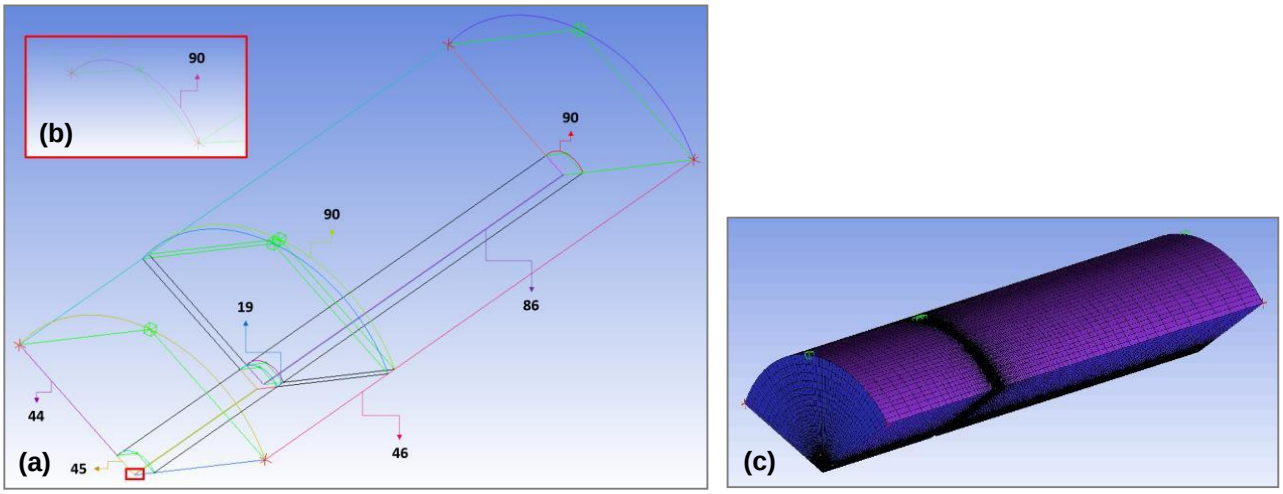

Figure 5: (a) Refinement of the ZE. (b) Rounding of the center edge of the domain. (c) SZ mesh. Source: Authors.

2.4.1 Mesh refinement

In order to obtain reliable values and, consequently, the best computational cost-effective mesh, a mesh independence study was carried out in the ZR. By varying the dimensions of the elements present in the parts of the blade, set by the software ANSYS Fluent Meshing® software, different meshes were obtained until the convergence criterion of 1% set for the relative Cp difference be reached, as can be seen in Table 1. The dimensions of the ZR faces were not varied and were set at 6mm, with the exception of the top of the ZR with 12mm. The number of prismatic layers was maintained at 8 and the dimension of the first layer was defined as 0.05mm.

The results of the simulations are also shown in Table 1 along with the relative percentage difference between the subsequent Cp's.

Table 1 – Mesh Independence Study

Mesh	Surface (mm)	Leading Edge (mm)	Trailing Edge (mm)	Tip (mm)	N° of Elements (mi)	Cp (-)	Relative Cp Difference
1	4,5	0,75	0,01	4,5	3,9	0,1476	-
2	3,0	0,5	0,05	2,0	7,6	0,1258	14,8%
3	3,0	0,2	0,05	1,0	10,9	0,1285	2,1%
4	2,0	0,075	0,05	1,0	13,8	0,1319	0,9%

By carrying out the simulations, Mesh 4 resulted in a *Cp* value that was 0.9% different to Mesh 3, so the study ended at this point. The parameters of Mesh 1 were defined based on the values used in the validation, and the following meshes were the result of refining these values, based on the visual result of the spatial discretization observed in the ANSYS Fluent Meshing® software. Table 1 shows a big difference between Mesh 1 and the others, with a relative difference of 14.8% in the *Cp* value between Mesh 1 and Mesh 2, which demonstrates the importance of the study performed, rather than just using values based on the validation. Therefore, as the convergence factor of 1% in the relative difference between *Cp's* was reached from Mesh 3 to Mesh 4, the study was finished and Mesh 4, with 13.8 million elements and a resulting *Cp* of 0.1272, was defined as the base mesh for describing the characteristic curve.

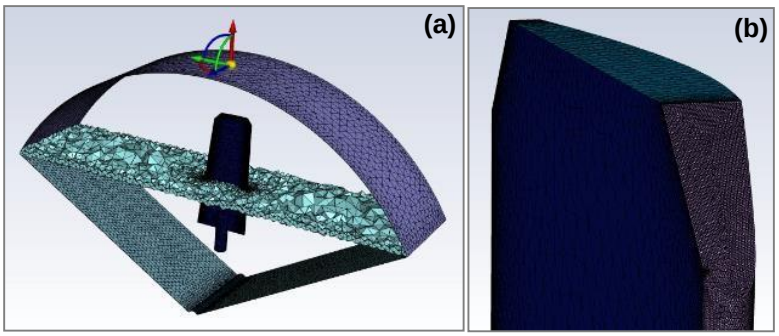

Figura 6: RZ mesh (a) and leading edge in details (b) with Mesh 4. Source: Authors.

However, the y+ values resulting from these simulations were not adequate, being around 5.0, much higher than 1. It was therefore necessary to carry out another mesh refinement study, but this time only on the boundary layer of the case. For this study, the number of prismatic layers and the size of the first layer were varied, and to define the best configuration, the values of *Cp*, y^+ and *GRV* were measured to guide the study. The data and results of the study can be analyzed in Table 2.

Table 2 – Boundary Layer Refinement Study

Malha	N° of layers	1^{st} layer dimension (mm)	N° of elements (mi)	*Cp*	y+	GRV
4.1	8	0,020	14,8	0,1106	1,516	0,0143
4.2	12	0,025	17,1	0,1027	1,428	0,0151
4.3	12	0,020	17,4	0,0794	1,166	0,0133
4.4	16	0,050	19,7	0,0127	0,964	–

Thus, after the simulations, the configuration that obtained the best *GRV* and especially y+ values, along with suitable *Cp* values, was the Mesh 4.3, with 12 layers and 0.020 mm dimension for the first layer. Mesh 4.4 obtained the best y+ value, being the only one below 1, which is the most recommended, but the resulting *Cp* was inadequate, inconsistent with the theory, and was therefore ruled out. So, the final *Cp*, y^+ and *GRV* values for the 5.33 *TSR* condition of the micro HAWT were 0.0794, 1.166 and 0.0133, respectively.

Beforehand, it can already be noted that considering the low *Cp* value found, this will probably not be the maximum *Cp* point of the curve, indicating a certain incompatibility with the experimental tests carried out, but this did not make it impossible to use them as a starting point

Finally, the base mesh got a total number of approximately 19.7 million elements and the quality metrics achieved were 0.83 for maximum skewness and 0.45 and 0.08 for minimum determinant and orthogonal qualities.

2.5 Solver Settings

The software used was ANSYS Fluent ®, where the pressure-based solver was used and in a permanent regime. The periodicity boundary condition was used from a moving reference frame (MRF). The turbulence model was the k-ω SST and the working fluid was air, with a constant density equal to 1.225 kg/m³. Using the coupled pressure-velocity coupling algorithm, the spatial discretization equations were configured as upwind, using the method based on least squares cell based for the gradients. In addition, the under-relaxation factors for density were defined as 0.45.

For the boundary conditions, the following settings have been specified:

- Wind velocity at the entrance: 5.92 m/s (value used on experimental analysis), constant, with turbulence intensityequal to 4% and representative length equal to the diameter of the wind tunnel flow redirector (in this case, 33 mm);
- Outlet pressure: 0 Pa (gauge), with turbulence intensity equal to 4% and representative length equal to the radiusof the blade (250 mm);
- Walls: zero slip condition on the upper face of the SZ and on the surface of the blade;
- Interfaces: interface condition on surfaces in contact with RZ and SZ;
- Periodic Faces: condition of rotational periodicity at 120° (1/3 of the rotor channel), of the conforming type, onthe lateral surfaces of the two subdomains;
- Center edge fillet faces: axis condition.

As a convergence criterion, the minimum order for the residuals of the transport equations was 10^{-3}, and the torque coefficient and the static pressure in the rotor were monitored. Besides that, the *GRV* and y^+ dimensionless numbers average values were calculated, in the RZ and on the blade surface, respectively, to assess the suitability of the mesh.

3. RESULTS AND DISCUSSION

Figure 8 shows the static pressure contours resulting from the simulation of the micro HAWT at TSR = 3, which was the condition that resulted the highest *Cp* value. From the color scale, it can be seen that the highest static pressure values are concentrated on the pressure side of the blade, and the lowest values for the entire blade surface are present on the leading edge of the suction side, the region which the greatest flow acceleration occurs.

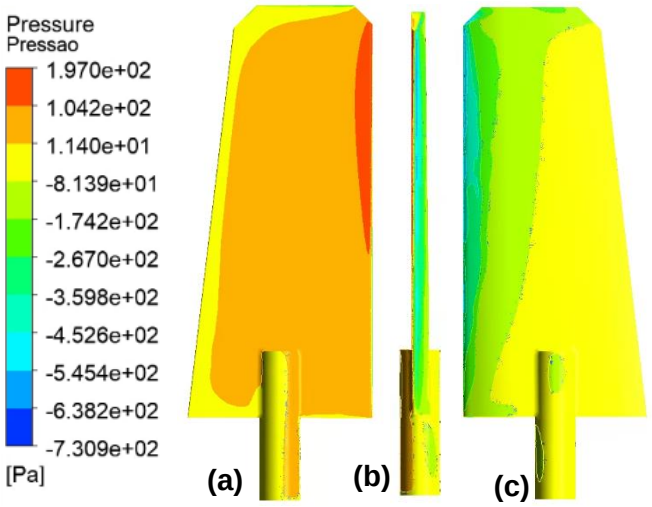

Figure 8 - Static pressure contours on the pressure side (a), suction side (b) and blade leading edge (c) (Authors).

Figure 9 shows the absolute velocity contours analyzed in a cross-section of the blade. It shows the presence of the lowest speeds in front of the turbine and in the wake area. In addition, the highest speeds are identified behind the turbine, especially near the leading edge, where the presence of a stagnation point stands out, the region that concentrates the highest absolute speed values measured.

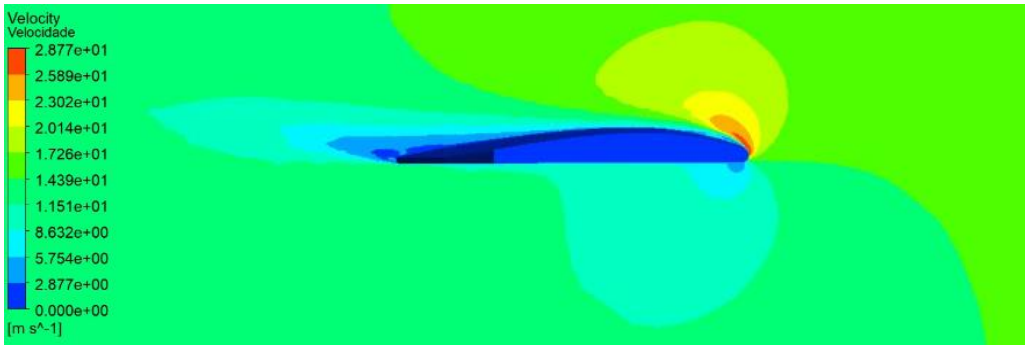

Figure 9 - Speed contours. Source: Authors.

It is interesting to note the correlation between Figures 8 and 9, because where the lowest pressures are observed, the highest speeds are also seen, which is consistent with the aerodynamic theory. Thus, the concepts of pressure side and suction side of the blade presented in Figure 8 are confirmed analogously in Figure 9 by the velocity contours, proving that the physics of the problem is coherent.

Figure 10 shows the effect of the turbine on the streamlines in the fluid domain. The aforementioned acceleration of the flow as it passes through the blades and the existence of a gradient for the circumferential velocity between the hub and the tip of the blade can be seen, proving the existence of the rotational movement of the turbine.

From the contours and streamlines in Figures 8, 9 and 10, it is possible to infer that the physics of the problem is correct. Due to the aerodynamic profile of the blade, the flow is accelerated, generating a low pressure zone behind the turbine, which characterizes the two sides of the blade, suction and pressure side. Therefore, the pressure gradient between the pressure and suction side of the blade it is responsible for the generation of the lift force that consequently produces

torque on the turbine axis.

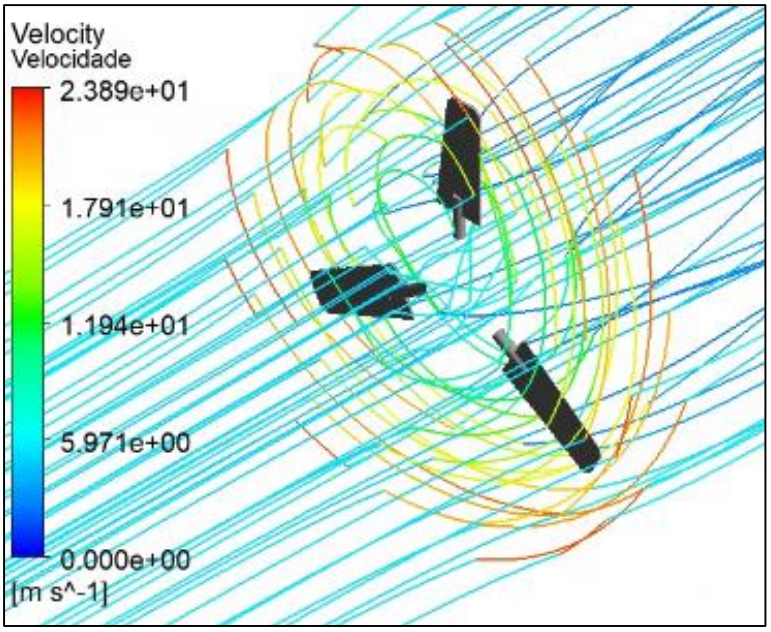

Figure 10 - Streamlines (Authors).

Figure 11 shows the described characteristic curve of the micro HAWT. Eight different speed conditions were simulated to describe the curve (at TSR of 2; 2.5; 3; 3.5; 4; 4.5; 5.33 and 7), 7 of them are shown in the graph. The *TSR* of 7.0 resulted on a *Cp* value close to 0.94, which is inconsistent as it exceeded Betz's limit of 0.59 by a certain degree. Therefore, this point is an outlier and was removed from the curve, but all the others, which obtained acceptable values and were consistent with the literature, were maintained. The shape of the curve looked as expected, with a maximum *Cp* of 0.3165 at a TSR of 3.0, something consistent with micro HAWTs and very close to the results obtained on the validation.

Using the points plotted on the graph to construct the curve, a 3rd degree regression was performed with a function equal to:

$$Y = -2.1087684 + 1.8390361 * X - 0.4584445 * X^2 + 0.0356796 * X^3 \quad (5)$$

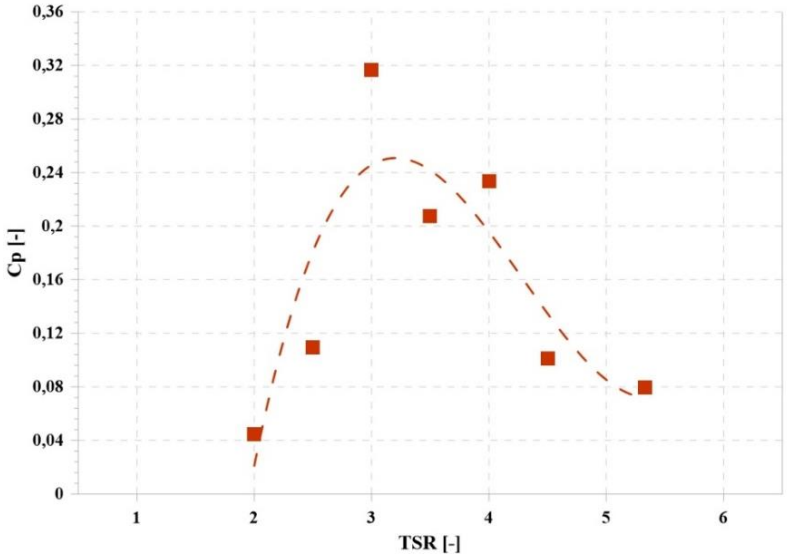

Figure 11 - Characteristic curve of the micro HAWT (Authors)

It is important to note that the analysis in question was carried out on a blade that does not have a registered aerodynamic profile and was simulated with a mounting angle equal to zero, so the expected value of coefficient of power, *Cp*, was low. For this reason and all the points mentioned, the values found are consistent and the analysis can be

considered valid.

The results of the *GRV* and y^+ calculations are shown in Figure 12. It is interesting to see the small variation in the number of *GRVs* and the almost linear growth in the y^+ values. For both cases, quadratic regressions were performed on the points measured.

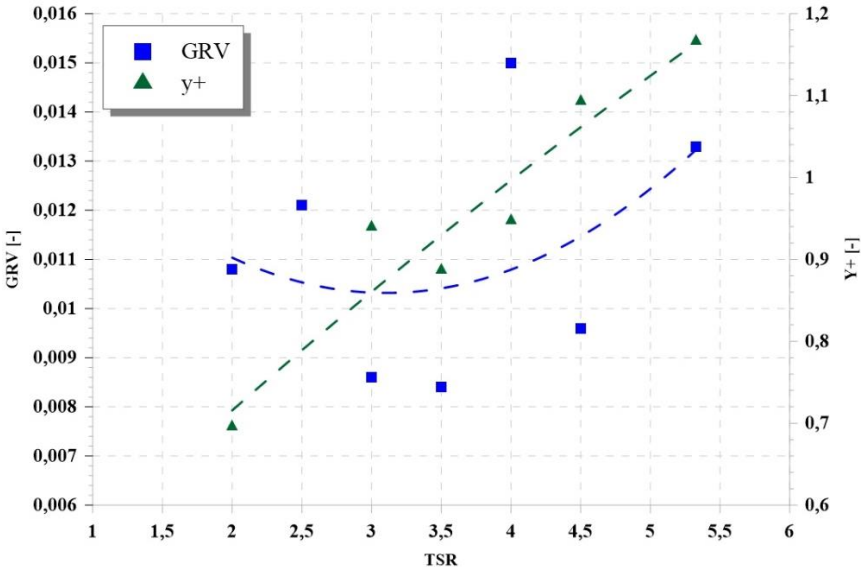

Figure 12 - Dimensional numbers (Authors)

After the adjustments made to the boundary layer, the final y+ values calculated were very appropriate. The y^+ value of 1.166, for the *TSR* = 5.33 condition, was actually the highest value measured. If this point really corresponded to the maximum Cp, it would be a little inappropriate for the y^+ to be greater than 1. However, as this is the highest TSR point on the curve described, it is acceptable that it only slightly exceeded the maximum recommended value of 1. Furthermore, only in two rotation conditions was the y^+ value greater than 1, and the lowest *TSR* had a very low value, of 0.7. Thus, based on the values calculated, it can be said that the problem's boundary layer was well discretized and is not a possible source of error in the simulation.

Just as a curiosity, the y^+ value obtained for the *TSR* = 7 simulation, which resulted in a *Cp* greater than 0.9, was 1.47.

As for the number of *GRVs*, the average values calculated were around 0.0111, which is very much in line with what was seen in the validation, where the average was also very close to this value. Compared to the validation results, the number of *GRVs* had a smaller variation in their calculated values for each *TSR*, which is interesting and indicates that the suitability of the mesh was similar between the simulations. However, unlike the validation of the methodology, there was no decrease in the *GRV* values as the speed increased, and the highest value was obtained at a *TSR* of 4.0.

It is also interesting to note that there is no reference value in the literature for the application of the *GRV* number in HAWT simulations in general, but the reference value for VAWT is in the order of 0.01, which is a good indication that the values measured are not incoherent and, furthermore, may even be an indication that for HAWT simulations the reference value for the dimensionless *GRV* is also close to 0.01.

4. CONCLUSION

In the present work a practical methodology for prediction of the aerodynamic performance of small HAWTs through the description of its characteristic curves has been developed. The methodology was validated by a relevant work in the literature and was complemented with the implementation of dimensionless numbers. So, the methodology was applied on the micro HAWT from the Laboratory of Renewable Sources and Solar Energy of the Federal University of Itajubá and was able to predict its aerodynamic performance in a fast way.

The use of dimensionless numbers had the goal to assess the suitability of the mesh and it also was effective in speeding up the discretization process of the problem and increasing the reliability of the results obtained. The *GRV* and y^+ dimensionless numbers data guided the mesh refinement study, indicating the best configurations, based on the prediction of the velocity gradients and the adequate discretization of the blade boundary layer, respectively.

The present study can be used in the future to help describing the best value for *GRV* number applied on micro HAWTs simulations and, for now on, this methodology can be applied on any HAWT of similar scale and could be used on wind energy microgeneration projects of many purposes, as for the application in remote regions of Brazil, to generate power and improve the life quality of the people who live in these places.

5. ACKNOWLEDGEMENTS

We thank the Minas Gerais State Research Support Foundation (FAPEMIG), PROCESS APQ-00653-22, referring to the project: "Numerical and Experimental Analysis of Wind Microgenerators for Applications in Remote Regions in Brazil", call 01/2022, registration at DPI UNIFEI No: PVDI297-2022, for funding this research. In addition, we thank PIBIC (Institutional Program for Scientific Initiation Scholarships), CNPq (National Council for Scientific and Technological Development) and PPGEEN (Postgraduate Program In Energy Engineering) for financial support and the Federal University of Itajubá (UNIFEI).

6. REFERENCES

Assembleia Geral da ONU. "Declaração Universal dos Direitos Humanos". "Nações Unidas", 217 (III) A, 1948, Paris, art.

F. Balduzzi, A. Bianchini, G. Ferrara, and L. Ferrari, “Dimensionless numbers for the assessment of mesh and timestep requirements in CFD simulations of Darrieus wind turbines,” Energy, vol. 97, pp. 246–261, Feb. 2016, doi: 10.1016/J.ENERGY.2015.12.111.

IEA, 2017, "Energy Access Outlook 2017: From poverty to prosperity".

IEA, 2018, "Statistics". Disponível em: < https://www.iea.org/statistics/statisticssearch/>.

GIFFORD, Mary Louise. A Global Review of Cookstove Programs. Dissertação de Mestrado da Universidade da California em Bekeley, California, 2010.

HSIAO, F. BIN; BAI, C. J.; CHONG, W. T. The Performance Test of Three Different Horizontal Axis Wind Turbine (HAWT) Blade Shapes Using Experimental and Numerical Methods. Energies 2013, Vol. 6, Pages 2784-2803, v. 6, n. 6, p. 2784–2803

IRENA [International Renewable Energy Agency] Renewable Power Generation Costs in 2018, 2019, Abu Dhabi. ISBN978-92-9260-126-3

Murali A, Rajagopalan RG. Numerical simulation of multiple interacting wind turbines on a complex terrain. J Wind EngInd Aerod 2017;162:57e7

RASAM, A. et al. Detached-eddy simulation of a horizontal axis wind turbine. Notes on Numerical Fluid Mechanics andMultidisciplinary Design, v. 137, p. 357–367, 2018.

SHIRZADEH AJIRLO, K. et al. Development of a wind turbine simulator to design and test micro HAWTs. SustainableEnergy Technologies and Assessments, v. 43, p. 100900, 1 fev. 2021.

Stathopoulos T, Alrawashdeh H, Al-Quraan A, Blocken B, Dilimulati A, Paraschivoiu M, Pilay P. Urban wind energy: some views on potential and challenges. J Wind Eng Ind Aerod 2018;179:146e57.

P. F. S. Trentin, P. H. B. de B. Martinez, G. B. dos Santos, E. E. Gasparin, and L. O. Salviano,Screening analysis and unconstrained optimization of a small-scale vertical axis wind turbine, Energy, vol. 240, p. 122782, Feb.2022, DOI: 10.1016/J.ENERGY.2021.122782.

Werlang A.B.C.; Geller I. Uma Análise da Relação Entre o Consumo de Energia Elétrica e o Crescimento Econômico Mundial. Universidade Federal do Rio de Janeiro - UFRJ, 2018.

7. RESPONSIBILITY NOTICE

The authors are the only responsible for the printed material included in this paper.